Research Article | Vol. 28, No. 6 / 16 March 2020 / Optics Express 7898
Optics EXPRESS

Terahertz-frequency temporal differentiator enabled by a high-Q resonator

JINGYA XIE,[1,2] XI ZHU,[1] HONGXIANG ZHANG,[1] XIAOFEI ZANG,[1] LIN CHEN,[1] ALEXEY V. BALAKIN,[3,4] ALEXANDER P. SHKURINOV,[3,4] AND YIMING ZHU[1,2,*]

[1]*Terahertz Technology Innovation Research Institute, Terahertz Spectrum and Imaging Technology Cooperative Innovation Center, Shanghai Key Lab of Modern Optical System, University of Shanghai for Science and Technology, Shanghai 200093, China*
[2]*Shanghai Institute of Intelligent Science and Technology, Tongji University, Shanghai 200092, China*
[3]*Faculty of Physics and International Laser Center, Lomonosov Moscow State University, Leninskie Gory 1, Moscow 19991, Russia*
[4]*ILIT RAS – Branch of the FSRC «Crystallography and Photonics» RAS, Svyatoozerskaya 1, 140700 Shatura, Moscow Region, Russia*
[*]*ymzhu@usst.edu.cn*

Abstract: Terahertz (THz) fundamental "building blocks" equivalent to those used in multi-functional electronic circuits are very helpful for actual applications in THz data-processing technology and communication. Here, we theoretically and experimentally demonstrate a THz temporal differentiator based on an on-chip high-quality (Q) factor resonator. The resonator is made of low-loss high-resistivity silicon material in a monolithic, integrated platform, which is carefully designed to operate near the critical coupling region. The experiment demonstrates that the device can perform the first-order time derivative of the input signal electric field complex envelope at 214.72 GHz. Our investigation provides an effective approach for terahertz pulse re-shaping and real-time differential computing units.

1. Introduction

Terahertz (THz) radiation, with the wavelengths between the infrared and microwave, is typically referred to as the frequencies from 0.1 THz to 10.0 THz [1,2]. Over the past few decades, with the rapid development of generation and detection of THz signals, various applications of THz have been found in non-destructive evaluation, biology and medical sciences, information and communication, and so on [3–8]. In addition to providing more complex THz systems, THz equivalents of fundamental devices that form basic building blocks in electronic and photonic circuits would need to be designed and implemented, such as arbitrary waveform generation, temporal integration and Hilbert transformer etc. [9–12]. These functions are basic building blocks of a general-purpose signal processor for signal generation and fast computing, which are very important for high-speed THz characterization and measurement. Temporal differentiator is one of these fundamental devices that performs the mathematical operation of differentiation. Given an arbitrary input signal in the time domain, it can provide the output derivative signal. Several methods have been proposed to realize the optical differentiator [13–16]. However, to the best of our knowledge, THz temporal differentiator has not been demonstrated. The main reason is that the temporal differentiator is extremely sensitive to variations of device parameters which must be fixed to satisfy very specific conditions. To achieve such high performance THz devices, the fabrication is challenging.

Recently, there has been a significant surge of progress in enabling high-performance THz resonators [17–23]. Integrated resonators can be used to realize the differentiator [24–31] and integrator [32,33], which are more suitable for a densely circuit in the optical domain. In this

#387775 https://doi.org/10.1364/OE.387775
Journal © 2020 Received 10 Jan 2020; revised 20 Feb 2020; accepted 22 Feb 2020; published 2 Mar 2020

Optics EXPRESS

paper, we present a THz temporal differentiator based on a silicon ring resonator and investigate its performance. The resonator is made of low-loss high-resistivity Si material in a monolithic, integrated platform, which is carefully designed to operate near the critical coupling region. Our device performs the first-order time derivative of the input signal electric field complex envelope at 214.72 GHz with a time resolution of 35 μs, corresponding to a processing bandwidth of ~10 KHz. The differentiation operation can be used directly in signal positive-going or negative-going slope recognition. This technology could provide a potential cost-effective solution for ultrafast pulse shaping, waveform generation, advanced coding and pulse characterization in THz communications.

2. Operation principle

A basic first-order differentiator is a linear filtering device that provides the first-order time derivative of the input signal electric-field complex envelope. This device can be implemented using a linear optical filter with a required spectral transfer function [34]. Figure 1 shows the operating principle of the optical temporal differentiator (OTD), The OTD can be regarded as a band filter to perform effective filtering calculation on the incoming optical signal.

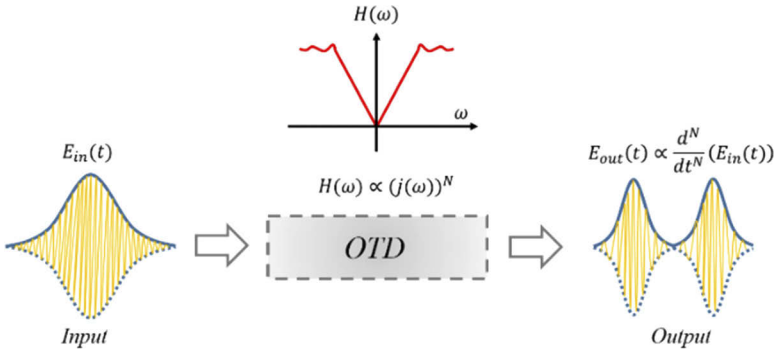

Fig. 1. A schematic of a first-order ($N = 1$) optical temporal differentiator.

For the modulated light from a continuous-wave source, the carrier angular frequency is ω_c. $s(t)$ is the input modulating signal. The optical field expression can be written as

$$E_{in}(t) = s(t)\exp(j\omega_c t) \tag{1}$$

The Fourier transform of the above function can be expressed as

$$E_{in}(t) = F\{(s(t)\exp(j\omega_c t))\} = S(\omega - \omega_c) \tag{2}$$

where $S(\omega)$ is the Fourier transform of $s(t)$. If we differentiate the complex amplitude of the input optical signal by the Nth order, then the output signal expression is

$$E_{out}(t) = \frac{\partial^N s(t)}{\partial t^N}\exp(j\omega_c t) \tag{3}$$

where N is differentiation order which is a fraction or integer. The Fourier transform of the output signal can be written as

$$E_{out}(\omega) = F\left\{\left(\frac{\partial^N s(t)}{\partial t^N}\exp(j\omega_c t)\right)\right\} = (j(\omega - \omega_c)^N S(\omega - \omega_c)) \tag{4}$$

Combining Eqs. (2) and (4), we see that differentiating the complex amplitude of the output signal is equivalent to multiplying the spectrum of the input signal by a transfer function

Optics EXPRESS

$(j(\omega\text{-}\omega_c))^N$. Therefore, the transfer function of an ideal optical field differentiator is as follows

$$H_{ideal}(\omega) = (j(\omega - \omega_c))^N \tag{5}$$

According to Eq. (5), the amplitude spectral response is proportional to $|\omega\text{-}\omega_c|^N$ ($N = 1, 2, 3, \ldots$). The spectral phase response for an even-order differentiator has a linear profile. For an odd-order differentiator, there is an additional discrete π-phase shift at the differentiator's central frequency (ω_c). As evidenced by the frequency transfer function $H(\omega)$, a differentiator is a notch optical filter (i.e. a band-stop filter) which provides the Nth derivative of the temporal complex envelope of the input optical signal.

3. Numerical analysis of terahertz ring resonator (TRR) differentiator

In order to achieve a notch THz filter, we demonstrate a ring resonator device. It consists of a ring waveguide as a resonant cavity, which is evanescently coupled with a single straight bus waveguide serving as the input and output port. The transfer function of the resonator can be expressed as

$$T = \frac{t - ae^{-j\beta L}}{1 - ate^{-j\beta L}} \tag{6}$$

where β=$2\pi n_{eff} f_c/c$ is the propagation constant of the resonator waveguide, t is the coupling coefficient and a is the field attenuation per round trip in the cavity, and L is the total perimeter of the terahertz ring resonator (TRR). According to Eq. (6), we can deduce that the depth and the bandwidth of the resonance is changing with the coupling regime, and consequently the amount of the phase shift could also been changed from less than π, to π and finally to greater than π. The black solid curves in Figs. 2(a) and 2(b) show the amplitude and phase response for the terahertz ring resonator 1 (TRR1) operating at the critical coupling region ($t = a$). A fully phase shift (π) is achieved and the Lorentz filter shape transmission is shown at the center of the resonance. The parameters used in simulations are identical to those in the experiment for comparison, except that a is a little bit different ($a = 0.941$). To prove the operation of the device, the blue dotted curves in Figs. 2(a) and 2(b) show the amplitude response and phase response of the ideal first-order differentiator (IFOD) at the resonant operating frequency. The figure shows that the Lorentz filter and IFOD have quite similar magnitude response, and both show a phase jump of π around central frequency (ω_c). Hence, the transfer function of a single side coupled silicon ring resonator operating at the critical coupling region can provide the required spectral features. The red dash curves in Fig. 2 show the response for the terahertz ring resonator 2 (TRR2). Its parameters are the same as the fitting results in Section 4 ($a = 0.933$, $t = 0.941$). The farther the resonance is from the critical coupling, the more response deviations there will be between the TRR and IFOD. In practice, deviations from the ideal conditions of ring resonator should be expected and this should affect the device operation as an optical differentiator, such as a non-zero resonance dip, non-abrupt phase jump, and inexact π phase shift.

In order to investigate the proper performance of the designed temporal differentiator, we have numerically simulated the time-domain response of the critical coupling TRR1. The calculations are based on the operation principle discussed in Section 2. The input square waveform is shown in Fig. 3 by the red dash curve. The repetition rate of square waveform signal is 100 KHz. The rising and falling time (defined as the time that the pulse amplitude increases or decreases from 10% to 90%) T_0 is set to be 0.12 μs as a test case. The black-solid curve in Fig. 3 shows the output of the optical differentiator. All signals have been normalized in amplitude in order to facilitate the comparison between them. It can be seen the differentiation of a square pulse results in two impulses at the rising and falling edges.

Optics EXPRESS

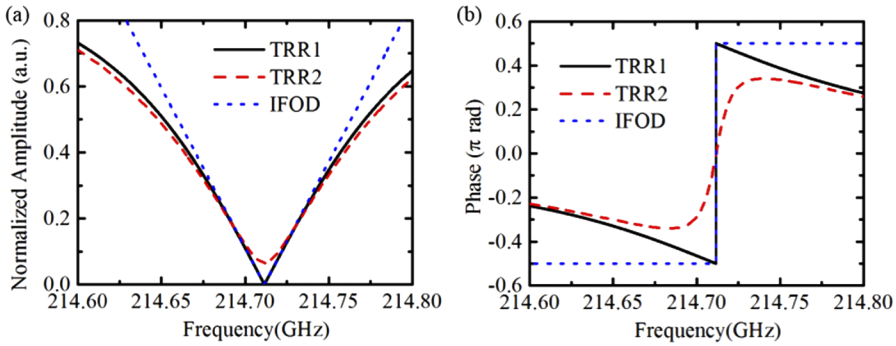

Fig. 2. (a) Amplitude response of the IFOD (blue-dotted curve), the critical coupling TRR1 (black-solid curve) and the non-critical coupling TRR2 (red-dashed curve) at the resonant operating frequency. (b) Corresponding phase response.

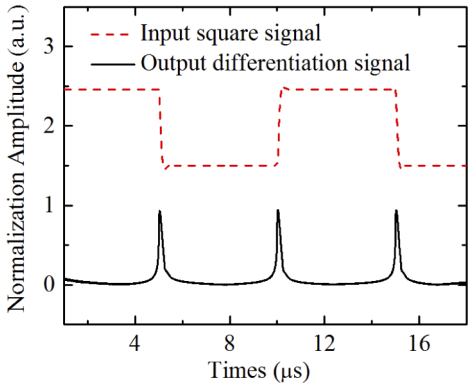

Fig. 3. Temporal waveforms of the input square wave (red-dashed curve) and the output differentiation result (black-solid curve).

4. Experimental results and discussion

We fabricated the TRR differentiator on a low-loss high-resistivity silicon wafer using complementary metal-oxide semiconductor (CMOS) compatible fabrication processes. The device is fabricated on a double-sided polished silicon wafer with a thickness of 470 μm, which consists of a ring waveguide and a straight waveguide. The coupled ring structure is designed as a racetrack ring and the resonant mode is designed to operate near the critical coupling region. The waveguide mode is coupled into TRR from the adjacent waveguide. The bus and ring waveguides have the same width (W) of 500 μm. The waveguide height is $H = 340$ μm with a slab thickness (h) of 130 μm. The radius of the racetrack rings is $r = 3.25$ mm. The coupling length (L) is 1 cm given by the straight waveguide in the racetrack ring. The strength of coupling can then be lithographically controlled by adjusting the distance between the waveguide and the ring. Here, the gap (g) is chosen as 50 μm to achieve the critical coupling. To define the waveguide patterns, deep ultra-violet (DUV) photolithography was employed, followed by anisotropic dry etch of silicon. The etching depth is 340 μm, in accordance with the waveguide height. The fabricated ring resonator formed by the ridge-type waveguide in our experiment is a fully passive device.

To investigate the characterization of the fabricated THz temporal differentiator, we measured the transmission and phase spectra of the device for the transverse magnetic (TM) polarization (electric field perpendicular to the device plane). For this purpose, we used the method described in [19]. The system employs an Agilent N5227A PNA network analyzer and a pair of WR-5.1

Optics EXPRESS

140-220 GHz VNA extenders. Figure 4(a) shows the transmission spectrum of this device in the frequency band from 206 GHz to 216 GHz. The results show that the device we used here is a resonator with a FSR of 1.7984 GHz. Figure 4(b) shows the detailed power transmission and phase spectra around the resonance dip. The resonance dip was centered at 214.72 GHz, and exhibited a transmission extinction ratio of 22 dB, as shown by the black dotted-dashed curve. The Q factor of resonator is ~2385. The measured spectral phase response is shown by the blue sold line. As expected, a relatively abrupt phase shift 0.97 π (close to π) was obtained. The red dotted line and pink dashed line is the fitted transmission spectrum and phase response with $a = 0.933$, and $t = 0.941$, respectively. Comparing the fitted model and the experiment result, there is a noticeable difference in the tails of the phase profile, we believe this discrepancy is caused by the strong Fabry-Perot resonance, which is visible in Fig. 4(a). According to Eq. (6), we know that in order to further increase the phase shift to π, t and a need to be in closer proximity to satisfy the critical coupling condition.

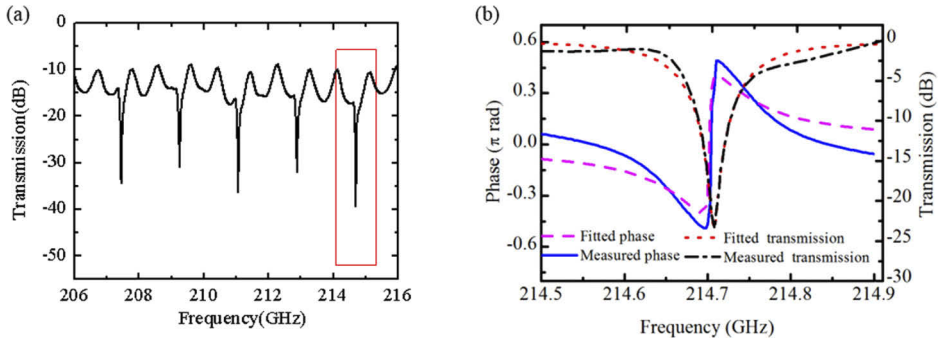

Fig. 4. (a) Measured transmission spectrum of the racetrack ring cavity device for TM mode in the frequency band of 206GHz-216 GHz. (b) Measured and fitted spectra of the resonance at 214.72 GHz.

To verify the features experimentally, we measured the fabricated TRR using the experimental setup shown in Fig. 5. The insets (a) and (b) are the schematic drawing of the TRR and cross-sectional view of waveguides, respectively. The desired waveform signal is generated by modulating a continuous wave using the external modulation mode of the radio frequency and microwave signal generator (RF&MSG) driven by an arbitrary waveform generators (AWG). The AWG generates a periodic square wave at 1 KHz modulation rate. The frequency of the continuous wave is tuned to 11.925 GHz. After the signal generator extension module (SGX Module) with the multiplier of 18 times, the frequency of the carrier signal becomes 214.72 GHz (the resonant frequency). The power of output signal is about 0 dBm. The measured rising time of the signal is ~35 μs. The modulated electromagnetic wave signal is coupled into the bus waveguide of our device and the differential signal is coupled into the horn antenna (HA) from the right port of bus waveguide. Finally, we use a THz lens-coupled direct detector (DD) based on field-effect transistor to detect the temporal intensity profiles of the signals which are observed by a sampling oscilloscope (OSC).

Figures 6(a) and 6(c) show the normalized voltage amplitude profiles of the time-domain waveforms at the device output. The periodic square wave signal shown by the red-dashed line is acquired by tuning the frequency of the carrier signal from 214.72 GHz. When the operating frequency of carrier signal is tuned to 214.72 GHz (while other parameter setting stays the same), the voltage amplitude of the waveform is shown by the black-solid curve. As predicted, the experimental result is close to the analytical first-order temporal derivative of the input waveform shown in Fig. 3. Such design would allow us to get the rising and falling edge of the corresponding periodic square wave signal directly in the differential result, and meanwhile obtain a regular

Optics EXPRESS

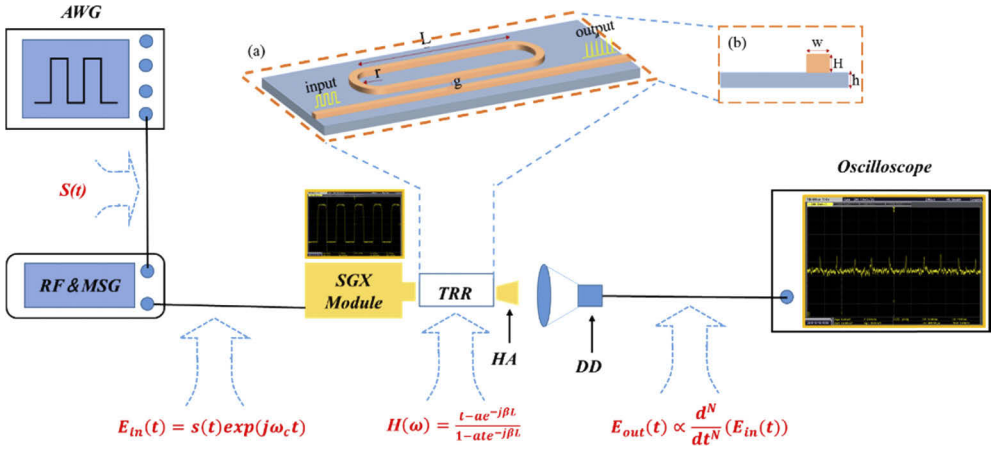

Fig. 5. Schematic of the experimental setup for measurements of THz integrated temporal differentiator. AWG: arbitrary waveform generators. RF&MSG: radio frequency microwave source. SGX Module: signal generator extension module. HA: horn antenna. DD: direct detector. The insets (a) and (b) are the schematic drawing of the TRR and cross-sectional view of waveguides, respectively.

high frequency pulse signal. The distortions of the differentiation signals could be resulted from the insufficient notch depth and inexact π phase shift of our device. The energetic efficiency, which could be measured as the ratio of average pulse powers between off-resonance output (input waveforms) and on-resonance output (differential waveforms) from the device, is close to

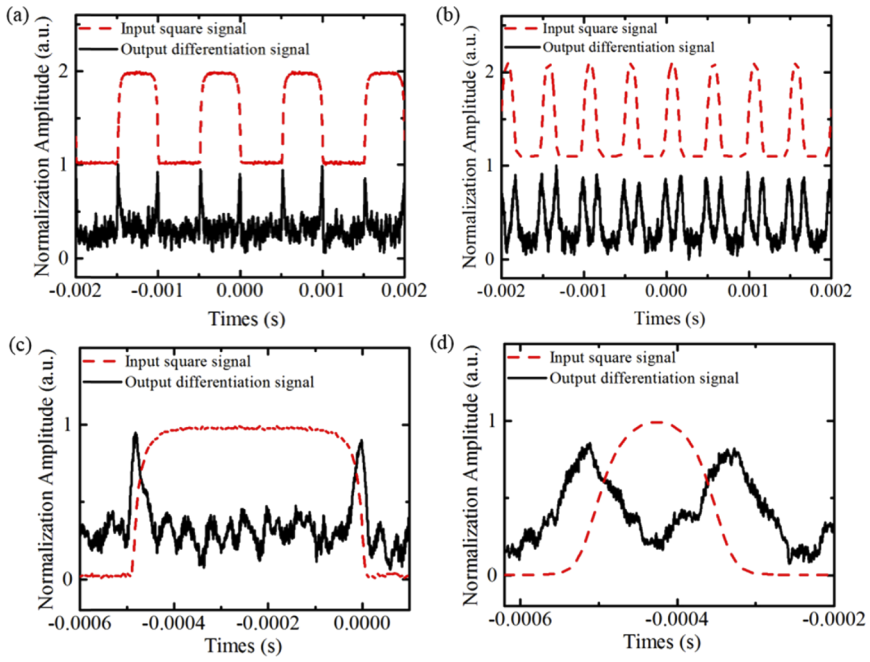

Fig. 6. (a) Experimental differential results of a square wave with a frequency of 1 kHz. (b) Experimental differential results of Gaussian pulse with pulse width of 100 μs. (c) and (d) show the detailed signals respectively.

Optics EXPRESS

0.11%. In addition, in order to test the versatility of our device differential function, Gaussian pulse waveform is used as the input signal. Theoretically, for an input of Gaussian pulses, an output of odd-symmetry Hermite-Gaussian pulses (OS-HG) is expected. Figures 6(b) and 6(d) show the experimental results of a Gaussian waveform (red-dashed line) with a pulse width of 100 μs and its first-order derivative (black-solid line). The repetition frequency is set to 2 KHz. The energetic efficiency is close to 0.59%. We can see that the differential effect of the Gaussian waveform is well obtained. Hence, above experimental results clearly demonstrate the THz differentiation functionality using this compact silicon device.

From Fig. 4, the 3 dB bandwidth of the TRR is around 90 MHz. According to the definition of device operation bandwidth (DOB) [34], the proposed THz temporal differentiator is expected to differentiate an input pulse with a bandwidth of tens of MHz, which is large enough for signal processing in our experiments. The bandwidth (BW) of the input square wave in the experiment is 10 kHz, which is related with the rising edge time: $BW = 0.35/T_{rise\ time}$ [35]. The bandwidth of the square wave after the frequency-multiplier is limited due to the limited bandwidth of SGX Module used in our experimental setup, which might be enhanced in the future work with improved experimental setup.

5. Conclusion

In summary, we proposed a THz temporal differentiator based on a silicon dielectric resonator. The performance of the differentiator is experimentally demonstrated with the periodic square wave signals and Gaussian pulses by a THz temporal measurement setup. This demonstration will pave towards the further exploration of THz signal processing function devices.

Funding

National Key Research and Development Program of China (2017YFA0701005); National Natural Science Foundation of China (61705131, 61671302, 61871268, 11604208, 11874266); Higher Education Discipline Innovation Project (D18014); Science and Technology Commission of Shanghai Municipality (17590750300); Ministry of Science and Higher Education (075-15-2019-1950); State assignment FSRC «Crystallography and Photonics» RAS.

Disclosures

The authors declare no conflicts of interest.

References

1. B. Ferguson and C. Zhang X, "Materials for terahertz science and technology," Nat. Mater. **1**(1), 26–33 (2002).
2. M. Tonouchi, "Cutting-edge terahertz technology," Nat. Photonics **1**(2), 97–105 (2007).
3. D. Zimdars, S. White J, G. Stuk, A. Chernovsky, G. Fichter, and S. Williamson, "Large area terahertz imaging and non-destructive evaluation applications," Insight (Northampton, U. K.) **48**(9), 537–539 (2006).
4. K. Ajito and Y. Ueno, "THz chemical imaging for biological applications," IEEE Trans. Terahertz Sci. Technol. **1**(1), 293–300 (2011).
5. K. Humphreys, P. Loughran J, M. Gradziel, W. Lanigan, T. Ward, A. Murphy J, and C. O'Sullivan, "Medical applications of terahertz imaging: a review of current technology and potential applications in biomedical engineering," in *Proceedings of IEEE Conference on Engineering in Medicine and Biology Society* (IEEE, 2004), pp. 1302–1305.
6. T. Nagatsuma, G. Ducournau, and C. Renaud C, "Advances in terahertz communications accelerated by photonics," Nat. Photonics **10**(6), 371–379 (2016).
7. W. M. Lee A and Q. Hu, "Real-time, continuous-wave terahertz imaging by use of a microbolometer focal-plane array," Opt. Lett. **30**(19), 2563–2565 (2005).
8. T. Chen H, J. Padilla W, M. Zide J, C. Gossard A, J. Taylor A, and D. Averitt R, "Active terahertz metamaterial devices," Nature **444**(7119), 597–600 (2006).
9. D. McKinney J, E. Leaird D, and M. Weiner A, "Millimeter-wave arbitrary waveform generation with a direct space-to-time pulse shaper," Opt. Lett. **27**(15), 1345–1347 (2002).

Optics EXPRESS

10. C. Koos, P. Vorreau, T. Vallaitis, P. Dumon, W. Bogaerts, R. Baets, B. Esembeson, I. Biaggio, T. Michinobu, F. Diederich, W. Freude, and W. Freude, "All-optical high-speed signal processing with silicon–organic hybrid slot waveguides," Nat. Photonics **3**(4), 216–219 (2009).
11. Y. Park, J. Ahn T, Y. Dai, J. Yao, and J. Azaña, "All-optical temporal integration of ultrafast pulse waveforms," Opt. Express **16**(22), 17817–17825 (2008).
12. H. Asghari M and J. Azaña, "All-optical Hilbert transformer based on a single phase-shifted fiber Bragg grating: design and analysis," Opt. Lett. **34**(3), 334–336 (2009).
13. M. Rivas L, S. Boudreau, Y. Park, R. Slavík, S. LaRochelle, A. Carballar, and J. Azaña, "Experimental demonstration of ultrafast all-fiber high order photonic temporal differentiators," Opt. Lett. **34**(12), 1792–1794 (2009).
14. M. Kulishov, D. Krcmarík, and R. Slavík, "Design of terahertz-bandwidth arbitrary-order temporal differentiators based on long-period fiber gratings," Opt. Lett. **32**(20), 2978–2980 (2007).
15. Y. Park, J. Azaña, and R. Slavík, "Ultrafast all-optical first-and higher-order differentiators based on interferometers," Opt. Lett. **32**(6), 710–712 (2007).
16. L. Zhang, J. Wu, X. Yin, X. Sun, P. Cao, X. Jiang, and Y. Su, "A high-speed second-order photonic differentiator based on two-stage silicon self-coupled optical waveguide," IEEE Photonics J. **6**(2), 1–5 (2014).
17. Z. Wang, S. Yuan, G. Dong, R. Wang, L. Chen, X. Wu, and X. Zhang, "On-chip single-mode high-Q terahertz whispering gallery mode resonator," Opt. Lett. **44**(11), 2835–2838 (2019).
18. W. Vogt D and R. Leonhardt, "Ultra-high Q terahertz whispering-gallery modes in a silicon resonator," APL Photonics **3**(5), 051702 (2018).
19. Y. Xie J, X. Zhu, F. Zang X, Q. Cheng Q, L. Chen, and M. Zhu Y, "Terahertz integrated device: high-Q silicon dielectric resonators," Opt. Mater. Express **8**(1), 50–58 (2018).
20. I. S. Amiri, F. Alizadeh, M. M. Ariannejad, R. Amini, and P. Yupapin, "Computation of ion exchange buried microring resonator waveguide for THz communication applications," Results Phys. **10**, 287–290 (2018).
21. S. Yuan, L. Chen, Z. Wang, R. Wang, X. Wu, and X. Zhang, "Mode coupling in a terahertz multi-mode whispering-gallery-mode resonator," Opt. Lett. **44**(8), 2020–2023 (2019).
22. Z. Wang, G. Dong, S. Yuan, L. Chen, X. Wu, and X. Zhang, "Voltage-actuated thermally tunable on-chip terahertz filters based on a whispering gallery mode resonator," Opt. Lett. **44**(19), 4670–4673 (2019).
23. W. Vogt D, H. Jones A, G. Schwefel H, and R. Leonhardt, "Prism coupling of high-Q terahertz whispering-gallery-modes over two octaves from 0.2 THz to 1.1 THz," Opt. Express **26**(24), 31190–31198 (2018).
24. F. Liu, T. Wang, L. Qiang, T. Ye, Z. Zhang, M. Qiu, and Y. Su, "Compact optical temporal differentiator based on silicon microring resonator," Opt. Express **16**(20), 15880–15886 (2008).
25. A. Zheng, J. Dong, L. Zhou, X. Xiao, Q. Yang, X. Zhang, and J. Chen, "Fractional-order photonic differentiator using an on-chip microring resonator," Opt. Lett. **39**(21), 6355–6358 (2014).
26. H. Shahoei, X. Xu D, H. Schmid J, and J. Yao, "Photonic fractional-order differentiator using an SOI microring resonator with an MMI coupler," IEEE Photonics Technol. Lett. **25**(15), 1408–1411 (2013).
27. J. Dong, A. Zheng, D. Gao, S. Liao, L. Lei, D. Huang, and X. Zhang, "High-order photonic differentiator employing on-chip cascaded microring resonators," Opt. Lett. **38**(5), 628–630 (2013).
28. B. Jin, J. Yuan, K. Wang, X. Sang, B. Yan, Q. Wu, F. Li, X. Zhou, G. Zhou, C. Yu, C. Lu, H. Y. Tam, and P. K. A. Wai, "A comprehensive theoretical model for on-chip microring-based photonic fractional differentiators," Sci. Rep. **5**(1), 14216 (2015).
29. G. Zhou, L. Zhang, F. Li, X. Hu, T. Wang, Q. Li, M. Qiu, and Y. Su, "All-optical temporal differentiation of ultra-high-speed picosecond pulses based on compact silicon microring resonator," Electron. Lett. **47**(14), 814–816 (2011).
30. H. N. Mardanqom, M. A. Khosroshahy, and E. N. Aghdam, "Design and Simulation of a Compact All-Optical Differentiator Based on Silicon Microring Resonator," Int. J. Eng. Sci. **6**(5), 82–86 (2017).
31. L. Lu, J. Wu, T. Wang, and Y. Su, "Compact all-optical differential-equation solver based on silicon microring resonator," Front. Optoelectron. **5**(1), 99–106 (2012).
32. M. Ferrera, Y. Park, L. Razzari, B. E. Little, S. T. Chu, R. Morandotti, D. J. Moss, and J. Azaña, "On-chip CMOS-compatible all-optical integrator," Nat. Commun. **1**(1), 29 (2010).
33. M. Ferrera, Y. Park, L. Razzari, B. E. Little, S. T. Chu, R. Morandotti, D. J. Moss, and J. Azaña, "All-optical 1st and 2nd order integration on a chip," Opt. Express **19**(23), 23153–23161 (2011).
34. R. Ashrafi and J. Azaña, "Figure of merit for photonic differentiators," Opt. Express **20**(3), 2626–2639 (2012).
35. L Teng H and H Yew Y, "Multi-port high bandwidth interconnect equivalent circuit model for 3.2 Gbps channel simulation," in *Proceedings of IEEE Conference on Electronics Packaging Technology* (IEEE, 2016), pp. 638–643.